Double constricted channel for laminar flow and heat transfer based on double MRT-LBM.

E.B. Lahmer[a*], M.A. Moussaoui[a], A. Mezrhab[a], V. Botton[b], D. Henry[b]

[a] Laboratory of Mechanics & Energy, Faculty of Sciences, Mohammed 1st University, 60000 Oujda, Morocco.
Email : lahmerelbachir@gmail.com, moussaoui.amine@gmail.com, amezrhab@yahoo.fr
[b] Laboratoire de Mécanique des Fluides et d'Acoustique, CNRS/Université de Lyon, Ecole Centrale de Lyon/Université Lyon 1/INSA de Lyon, ECL, 36 Avenue Guy de Collongue, 69134 Ecully Cedex, France
Email : valery.botton@insa-lyon, daniel.henry@ec-lyon.fr

Résumé :

Dans le présent travail, on étudie numériquement l'écoulement de fluide et du transfert de chaleur dans un canal bidimensionnel à double constriction. Les simulations ont été réalisées à l'aide de la méthode de Boltzmann sur réseau avec des temps de relaxation multiples. Le champ d'écoulement de fluide est déterminé par le modèle D2Q9, et le champ de température par le modèle D2Q5. Une étude bien détaillée a été réalisée pour interpréter l'effet de la partie serrée et la variation du nombre de Reynolds sur l'écoulement et le refroidissement des parois du canal. Les résultats sont présentés en termes de lignes de courant, d'isothermes et de nombre de Nusselt moyen.

Abstract:

This paper focuses mainly on the investigation of the fluid flow and convective heat transfer inside a two-dimensional double constricted channel employing the Lattice Boltzmann Method with multiple relaxation times (LBM-MRT). To describe the fluid behavior and the heat transfer, a detailed study was performed to interpret the effect of the constriction part and the Reynolds number variation using the D2Q9 and the D2Q5 model. A detailed study was performed to interpret the effect of the constriction part and the Reynolds number variation. The results are presented in the form of streamlines, isotherms and averaged Nussel number.

Keywords: fluid flow, heat transfer, lattice Boltzmann method-MRT, double constricted channel, laminar flow, incompressible flow, double MRT.

Nomenclature.

a	constant parameter, -4<a<1.
f, g	density distribution function.
f^{eq}, g^{eq}	equilibrium density distribution function.
h	constriction width, m.
H	channel width, m.
l	block height, m.
L	channel length, m.
Nu	Local Nusselt number.
Pr	Prandtl number, = ν/α.
Re	Reynolds number, =Re = 2. r.U_{in}.H/μ
T	temperature, K.
u,v	x,y-velocity components, ms^{-1}
w	distance between the first and the second constriction.
2h/H	constriction ratio.

Greek symbols.

α	thermal diffusivity, m^2s^{-1}
θ	dimensionless temperature, =T-T_{in}/T_w-T_{in}
μ	kinematic viscosity, m^2s^{-1}
ρ	density of fluid, $Kg.m^{-3}$
<Nu>	Average Nusselt Number.

Subscripts.

w	wall
in	inlet

1 Introduction.

New technologies related to the current generation of high-performance electronic devices had a great attention concerning the development of the electronic components efficiency and response speed. Concerning the cooling systems domain, Bar-Cohen [1] found that the increase of the optimal temperature of a silicon chip in certain electronic parts decreases their performance and reliability. Therefore, the general orientation of the current research focuses on the effectiveness improvement of the heat transfer by means of convective fluid flows in order to solve the engineering and industrial application fields [2-7]. The lattice Boltzmann method (LBM) is adopted instead of the conventional methods to simulate the Newtonian and non-Newtonian fluids behavior on the mesoscopic scale by introducing the BGK scheme for the collision operator [8-10]. Fortunately, the appearance of the multiple relaxation times (MRT) scheme proposed by D'Humières [11] makes it possible to remedy the viscous and thermal effect caused by the LBM-BGK scheme [10]. Thus, the LBM-MRT has been applied to simulate two dimensional fluid flows in double constricted channel. To investigate the thermal problem,

the thermal lattice Boltzmann models (TLBM) was employed to define the mechanism of the thermal fluid flow in different part of the channel. Among the models used and applied in different geometries, we can mention, the hybrid thermal lattice Boltzmann equation (HTLBE) employing the MRT model, the passive-scalar approach, and the double-populations using the SRT-BGK model [12-20]. Moussaoui et al. [13] studied the effect of the fluid flow and heat transfer on an obstructed channel using the Hybrid thermal lattice Boltzmann method (HTLBM). Keshtkar and Ghazanfari [16] employed the double-populations LBM-BGK approach to investigate the fluid flow and heat transfer inside a 2D enclosure with three hot obstacles. Li et al. [17] successfully simulated the natural convection for low Prandtl number fluids using the Double MRT thermal lattice Boltzmann method.

First, our simulation code has been validated with the results obtained by Gokaltun and Dulikravich [19]. Then, a global study was carried out to analyze the effect of the constricted width variation and Reynolds number on fluid flow and convective heat transfer.

2 Analysis and Modeling.

2.1 Physical and description problem.

The physical configuration of the present problem is illustrated in Figure 1. It consists of a double constricted channel where the height and the length are defined by H and L, respectively. For the constricted part, it is characterized by the constricted ratio $2h/H=0.6$ in which h and l are respectively, the height and the width for each block, and the distance between the first and the second constriction is w. The temperature of the bottom and the top walls is kept T_w=350K, and the temperature of the incoming fluid takes the value T_{in}=300K. Regarding the behavior of the fluid flow at the channel inlet, the velocity U_{in} and the temperature T_{in} profile is considered uniform to investigate two dimensional incompressible, viscous, laminar air flow (Pr = 0.708). At the outlet, the gradients of the velocity and temperature are set to zero. In fact, the Boussinesq approximation is taken into account to neglect the effects of the fluid compression according to following expression:

$$\rho = \rho_0 + \rho_T = \rho_0 + \beta(T_{in} - T_w) \tag{1}$$

The quantities ρ_0, β are the initial density and the thermal expansion, respectively. Thus, the studied fluid was approximately incompressible [22].

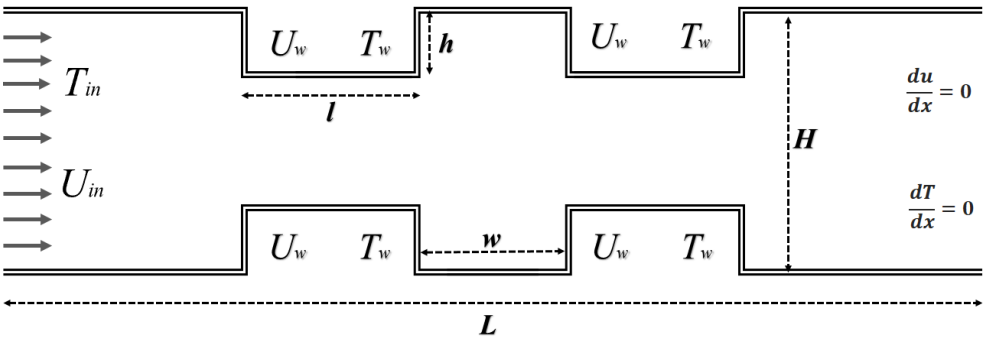

Figure 1: Schematic of the computational domain.

2.2 Numerical methods.

The LBM-MRT considered as a powerful numerical scheme in mesoscopic scale characterized by its accuracy, the simplicity and flexibility at the origin of reduced computation time compared to conventional CFD methods.

The simulation of the fluid flow and heat transfer based on LBM is mainly related to solving the Boltzmann equation that divided into two main expressions (advection and collision), this equation expresses the spatial-temporal evolution of the distribution function *fi* which represents the prospect of finding a particle density at a position $\boldsymbol{x}$ of space with a lattice speed $\boldsymbol{e_i}$ at a given time, as shown in the expression below:

$$f_i\left(\boldsymbol{x}+\boldsymbol{e}_i,t+1\right)-f_i\left(\boldsymbol{x},t\right)=\Omega_i(f) \quad i=0,...,8 \tag{2}$$

The operator Ω represents the collision part of the Boltzmann equation developed by D'Humières [11] using the LBM-BGK model [9]. To improve the computational instability problems for low viscosity caused by the SRT-LBM model [?], the D2Q9 multiple relaxation time Boltzmann equation (MRT-LBE) model is applied in this work to simulate the flow field (Fig.2). The evolution proposed by D'Humières to the collision operator makes it possible to write the following expression:

$$\boldsymbol{f}\left(\boldsymbol{x}+\boldsymbol{e},t+1\right)-\boldsymbol{f}\left(\boldsymbol{x},t\right)=-M^{-1}.S.\left(\boldsymbol{m}(\boldsymbol{x},t)-\boldsymbol{m}^{eq}(\boldsymbol{x},t)\right) \tag{3}$$

The matrix M indicates the 9×9 transformation matrix such as $m = M.f$, where m and f represent the moment vector and the distribution function, respectively, illustrated in the following expressions:

$m=(\rho,e,\varepsilon,j_x,q_x,j_y,q_y,p_{xx},p_{xy})^T$, $f=(f_0,f_1,f_2,f_3,f_4,f_5,f_6,f_7,f_8)^T$.

The notation T in the above expressions being the transport operator.

$$M=\begin{pmatrix} 1 & 1 & 1 & 1 & 1 & 1 & 1 & 1 & 1 \\ -4 & -1 & -1 & -1 & -1 & 2 & 2 & 2 & 2 \\ 4 & -2 & -2 & -2 & -2 & 1 & 1 & 1 & 1 \\ 0 & 1 & 0 & -1 & 0 & 1 & -1 & -1 & 1 \\ 0 & -2 & 0 & 2 & 0 & 1 & -1 & -1 & 1 \\ 0 & 0 & 1 & 0 & -1 & 1 & 1 & -1 & -1 \\ 0 & 0 & -2 & 0 & 2 & 1 & 1 & -1 & -1 \\ 0 & 1 & -1 & 1 & -1 & 0 & 0 & 0 & 0 \\ 0 & 0 & 0 & 0 & 0 & 1 & -1 & 1 & -1 \end{pmatrix} \tag{4}$$

The relaxation matrix S characterized by its relaxation rates s_i that define the elements of the diagonal matrix S in the moment space M , such as $S = diag\ (1.0, s_1, s_2, 1.0, s_4, 1.0, s_6, s_7, s_8)$. Regarding the moment vector m illustrated earlier in the above expression, can presented in the following elements order: the fluid density ($m_0 = \rho$), the kinetic energy (m_1 =e), the energy square ($m_{1=}\ \varepsilon\ =\ e^2$), $m_{3,5}=j_{x,y}$ are components of the momentum J=(j_x,j_y), the moment $m_{4,6}=q_{x,y}$ is related to the components of the energy flux, and the diagonal and off-diagonal components of the viscous stress tensor $m_{7,8}=p_{xx},_{xy}$.

After the collision step, the moments (m_0, m_3, m_5) conserve locally, whereas the moments (m_1, m_2, m_4, m_6, m_7, m_8) are conserving by taking into consideration the relaxation linearly towards their

equilibrium values using the relaxation equations for the non-conserved moments as shown in the expression below:

$$m^c = m + S \cdot (m^{eq} - m) \tag{5}$$

The moment m^c denotes the moment after collision, and the moment m^{eq} is the equilibrium moments such as:

$$m^{eq} = (\rho, e^{eq}, \varepsilon^{eq}, j_x, q_x^{eq}, j_y, q_y^{eq}, p_{xx}^{eq}, p_{xy}^{eq})^T \tag{6}$$

The equilibrium moments m^{eq} can develop them like:

$$\begin{aligned}
m_0^{eq} &= \rho \\
m_1^{eq} &= e^{eq} = -2\rho + 3(j_x^2 + j_y{}^2) \\
m_2^{eq} &= \varepsilon^{eq} = \rho - 3(j_x^2 + j_y{}^2)/\rho \\
m_3^{eq} &= j_x \\
m_4^{eq} &= q_x^{eq} = -j_x \\
m_5^{eq} &= j_y \\
m_6^{eq} &= q_y^{eq} = -j_y \\
m_7^{eq} &= p_{xx}^{eq} = (j_x^2 - j_y{}^2)/\rho \\
m_8^{eq} &= p_{xy}^{eq} = (j_x j_y)/\rho
\end{aligned} \tag{7}$$

To return to the speed space (f^c) from the moment space (m^c), the following equation can be used to prove this passage:

$$f^c = M^{-1} m^c \tag{8}$$

Where M^{-1} being the inverse matrix M.

The determination of the distribution functions f makes it possible to find the macroscopic fluid variables. Consequently, the density and the moment flux are obtained by the following equations:

$$\rho(\mathbf{x},t) = \sum_i f_i(\mathbf{x},t) \tag{9}$$

$$J(j_x, j_y) = \sum_i f_i(\mathbf{x},t)\mathbf{e}_i \tag{10}$$

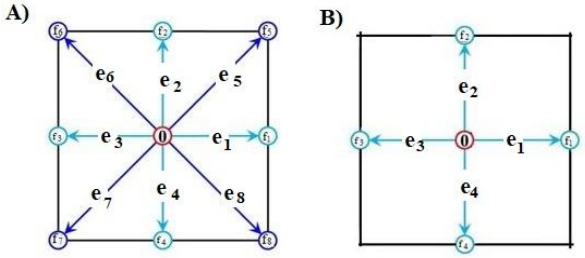

Figure 2: A) The two-dimensional D2Q9 velocity pattern B) The D2Q5 for thermal problem.

The studies applied in this field of calculation indicate that the use of the model D2Q9 for the thermal problem gives us the same results for the model D2Q5. Therefore, the D2Q5 model (Fig.2.) was applied in this work instead of the D2Q9 model to relieve the computational effort excessive applied by the MRT scheme in order to solve the heat transfer, and model the evolution of the energy conservation.

For the thermal problem, the distribution function g_i is written in the following way:

$$g_i(x + e_i, t + 1) - g_i(x, t) = \Omega_i(g) \qquad i = 0, \dots, 4 \tag{11}$$

As shown in the above equation, the advection-diffusion equation for the temperature field was solved by using a second set of a velocity distribution function $\{ g_i \in V(= R^5 | 0 \leq i \leq 4\}$. The collision operator Ω could be structured in the same way by introducing the MRT-TLBM model:

$$g_i(x + e_i, t + 1) - g_i(x, t) = M^{-1} \times S[m(x, t) - m^{eq}(x, t)] \tag{12}$$

Where M^{-1} denotes the inverse of transformation matrix for D2Q5 model obtained from the matrix M such as:

$$M = \begin{bmatrix} 1 & 1 & 1 & 1 & 1 \\ 0 & 1 & 0 & -1 & 0 \\ 0 & 0 & 1 & 0 & -1 \\ -4 & 1 & 1 & 1 & 1 \\ 0 & 1 & -1 & 1 & -1 \end{bmatrix} \tag{13}$$

The matrix M is orthogonal and invertible. The only conserved quantity is the temperature that can be determined by:

$$\theta = \sum_{i=0}^{N} g_i \tag{14}$$

where θ denote The dimensionless temperature, such as θ=(T-T_{in})/(T_w-T_{in}).
During the collision process, the non-conserved moments relax at different values corresponding to the equilibrium moment m^{eq} with taking into account the following relations presented below:

$$\begin{aligned} m_0^{eq} &= T \\ m_1^{eq} &= u \times T \\ m_2^{eq} &= v \times T \\ m_3^{eq} &= aT \\ m_4^{eq} &= 0 \end{aligned} \tag{15}$$

where the quantities (u, v) are the velocity field, and "*a*" is a constant parameter such as $a < 1$ in order to maintain the stability of the D2Q5 model. The relaxation matrix S characterized by the diagonal elements: $S = diag(1, s_\propto, s_\propto, s_e, s_v)$ such as the values of s_i is taken by the following values discussed in [20]:

$$s_\propto = \frac{6}{3 + \sqrt{3}} \; ; \quad s_e = s_v = \frac{3}{2} \tag{16}$$

The thermal diffusivity can be expressed according to the parameter *a* by the following relation:

$$\alpha = \frac{\sqrt{3}(4+a)}{60} \tag{17}$$

Also:

$$\alpha = \left(\frac{1}{s} - \frac{1}{2}\right)/5 \tag{18}$$

2.3 Velocity and thermal boundary conditions.

The introduction of the boundary conditions allows to determine the unknown distribution functions when the fluid particles hit the walls of the computational domain. Fortunately, the implementation of these boundary conditions is characterized by its simplicity and flexibility of integrating into the simulation code. The Zou & He boundary conditions [21] are employed to define the inlet and the outlet domain flow, and the bounce-back boundary conditions are employed to describe the solid walls of constricted channel [10].

To determine the thermal boundary conditions, it is necessary to move from the macroscopic scale to the mesoscopic scale which is related to the general term of the distribution function g_i as indicated in the following expressions [20]:

$$\mathrm{g_j} = \sum_{\mathrm{k=0}}^{4} (\mathrm{M^{-1}})_{\mathrm{jk}} \mathrm{m_k} \tag{19}$$

And:

$$\mathrm{g_1 + g_3} = 2\mathrm{T}\left(1 + \frac{\mathrm{a}}{4}\right)/5 \tag{20}$$

The equations illustrated above enable us to define the lower and upper thermal boundaries, respectively, $\mathrm{g_2} = \mathrm{g_4} + 2\theta_{\mathrm{w}}\left(1 + \frac{\mathrm{a}}{4}\right)/5$ and $\mathrm{g_4} = \mathrm{g_2} + 2\theta_{\mathrm{w}}\left(1 + \frac{\mathrm{a}}{4}\right)/5$, also the inlet domain flow, $\mathrm{g_1} = \mathrm{g_3} + 2\theta_{\mathrm{in}}\left(1 + \frac{\mathrm{a}}{4}\right)/5$ [18]. For the channel outlet, a second order extrapolation is used to obtain the unknown distribution functions $\mathrm{g_3(L,t)} = 2\mathrm{g_3(L-1,t)} - \mathrm{g_3(L-2,t)}$ [5].

2.4 Local and average Nusselt number formula.

The local Nusselt number can be expressed by the following formula:

$$Nu = \frac{L_c}{T_w - T_b} \frac{\partial T}{\partial n}\bigg|_{wall} \tag{21}$$

Where L_c denotes the characteristic length, and *n* being the normal to the studied surface (channel walls). The average Nusselt number is defined by the following expression:

$$< Nu >= \frac{1}{L_c} \int_{wall\ zone} Nu\ dn \tag{22}$$

3. Numerical Results.

3.1 The mesh independency study.

A preliminary study was carried out to find the most reliable mesh which corresponds to a high accurate results and an optimal calculation time. As shown in Figure 3, different meshes have been chosen for Re = 150 to define the optimal mesh to use.

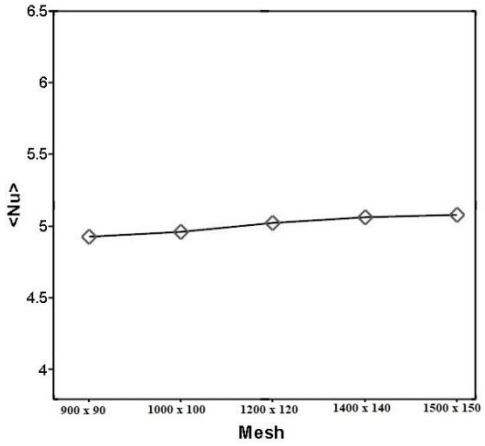

Figure 3: Computation of the average Nusselt number for different mesh (Re=150).

Let us note that the last three meshes 1200×120, 1400×140, and 1500×150 had very low relative errors for <Nu> which are 1.16%, 0.76%, and 0.36% respectively. Consequently, the 1400 × 140 mesh was chosen for all simulations achieved in this study.

3.2 Validation of the simulation code.

To validate our computer code was validated with the published results by Gokaltun and Dulikravich [19]. As illustrated in Figures 4 and 5, the velocity contours and the temperature fields for Re=10 are realized and compared with the finite element method (FEM) and lattice Boltzmann method for a single relaxation time (LBM-SRT) [19]. The results are compatible and satisfactory to find the results obtained in the paper [19]. Thus, the present simulation code is able to simulate our problem. After a preliminary study on the best mesh that can describe the phenomenon mentioned above, we have noted that the optimum grid used is 450×90.

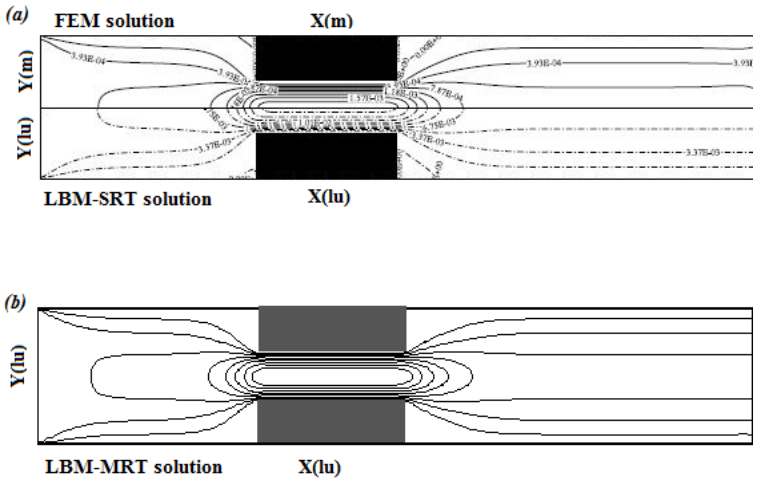

Figure 4: Velocity contours for Re=10: a) ref [19], b) current study.

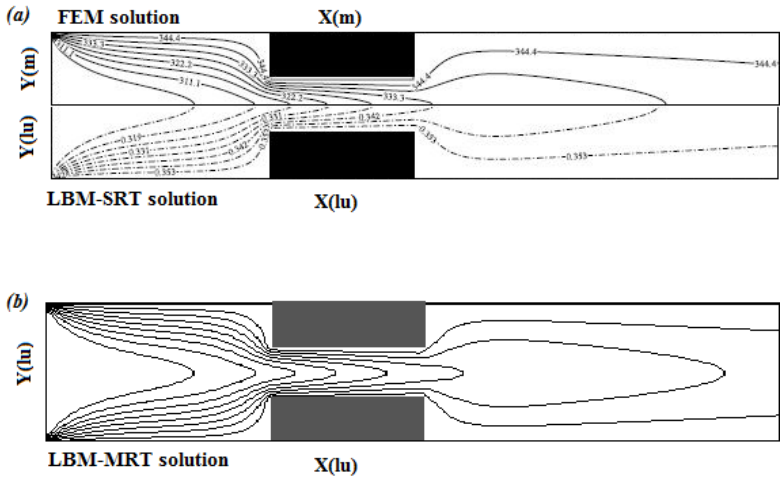

Figure 5: Temperature field for Re=10: a) ref [19], b) current study.

In addition, the average Nusselt number was investigated to cognize the rapprochement between the present study and the results of Gokaltun and Dulikravich [19]. As illustrated in Figure 6, there is a relevance between the two results for different values of the Reynolds number, which ensures a greater accuracy of our simulation code.

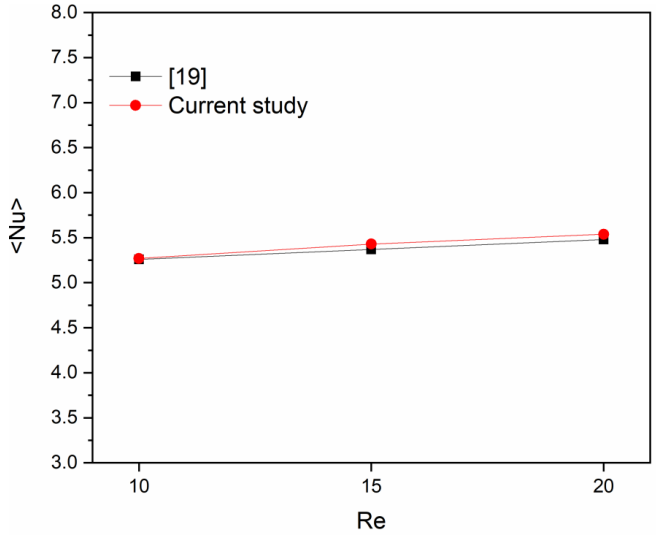

Figure 6: Validation of the average Nusselt number for various Reynolds number.

3.3 Results and Discussion.

In order to understand the mechanism of the fluid flow and the heat exchange effect between the fluid and the channel walls, a present study was performed for various values of Reynolds number ranged between 50 and 300 for constriction ratio equal 0.6. As shown in Figure 7, the fluid velocity is weak at the upstream and the downstream of the constricted regions, while the fluid velocity rises between the constricted zones, and a recirculation zones installed at the downstream of each these blocks. As the Reynolds number increases from 50 to 150, the fluid velocity increases and the recirculation zone strongly dominated behind the second strangled portion. Besides, the wake shape increases between the first and the second constricted. In the case when the Reynolds number reaches the value 250 and 300, the fluid flow becomes turbulent, and the recirculation zone becomes very intense at the downstream of the constriction channel. One can conclude that the appearance of the turbulent regime depending on the increase of the Reynolds number, and the inertial effects prevail on the viscous effects.

Concerning the thermal field, Figure 8 illustrates the temperature contours for each value of Reynolds number. At Re=50, the fluid is partially retained its initial temperature before the constricted region and completely heated after the constricted parts. When the Reynolds number reaches the value 150, the incoming fluid is totally maintained the initial temperature compared to the previous case, and the heat exchange between the fluid and the walls is also remarkable after the constricted zones. Despite the fact that the heat exchange is very high for low Reynolds numbers, the weakness of fluid flow decrease the heat transfer enhancement, while the heat transfer is improving for a high Reynolds number. When the turbulent regime is reached for Reynolds number equal 250 and 300, a deformation was observed at the downstream and the temperature contours loses its symmetry such as the heat transfer increases on the lower wall for Re=250 contrary to what found for Re = 300.

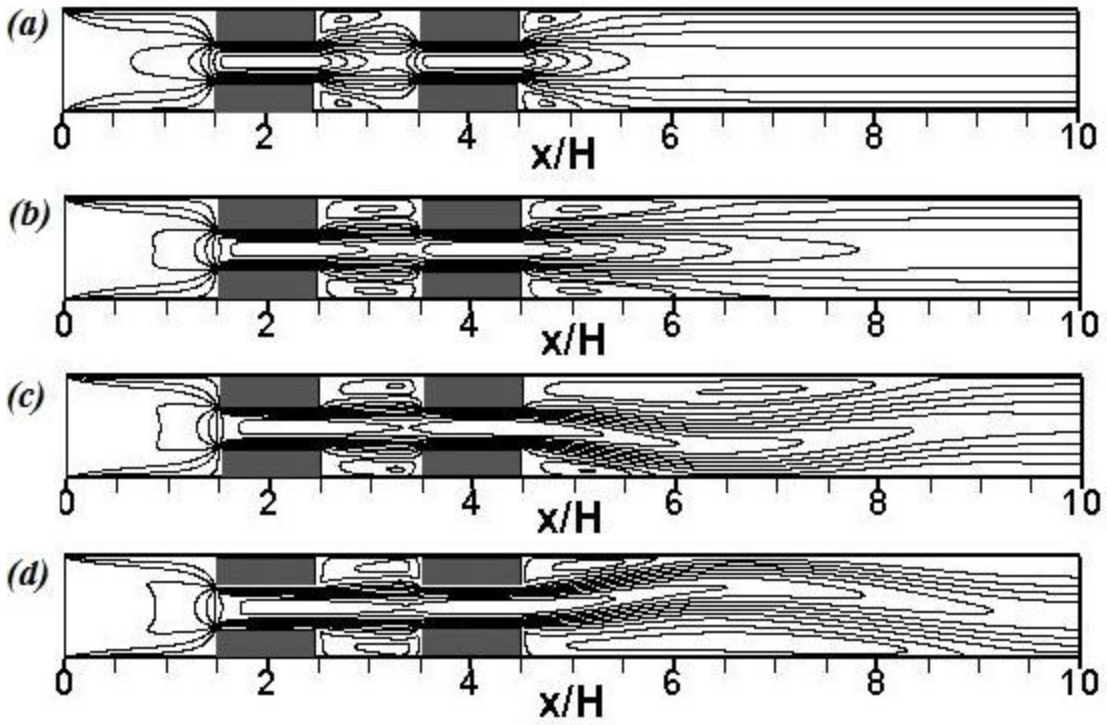

Figure 7: Velocity contours for constriction ratio 2h/H=0.6, a) Re=50, b) Re=150, c) Re=200, d) Re=300,

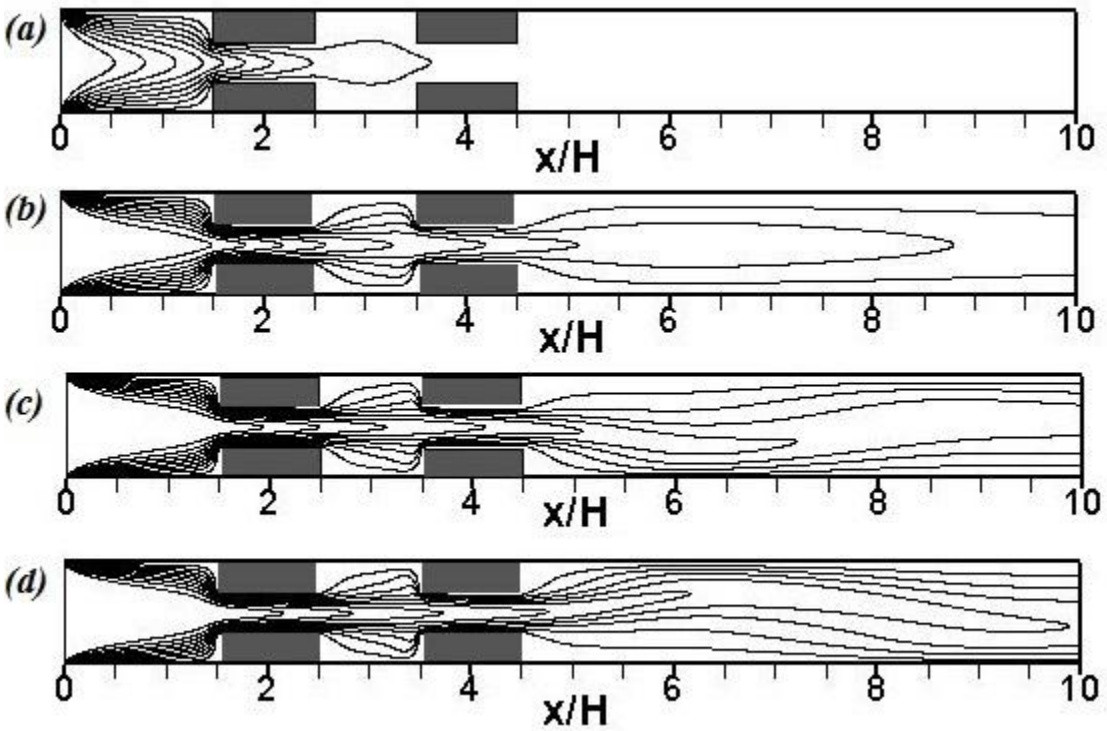

Figure 8: Temperature contours for 2h/H=0.6: a) Re=50, b) Re=150, c) Re=250, d) Re=300.

As a second study, the Reynolds number fixed to 250, and the constriction ratio varied from 0.2 to 0.5. The figure 9 shown the effect of the constriction ratio on the velocity contours, the fluid velocity increases when the constriction ratio raised and the recirculation becomes very remarkable.

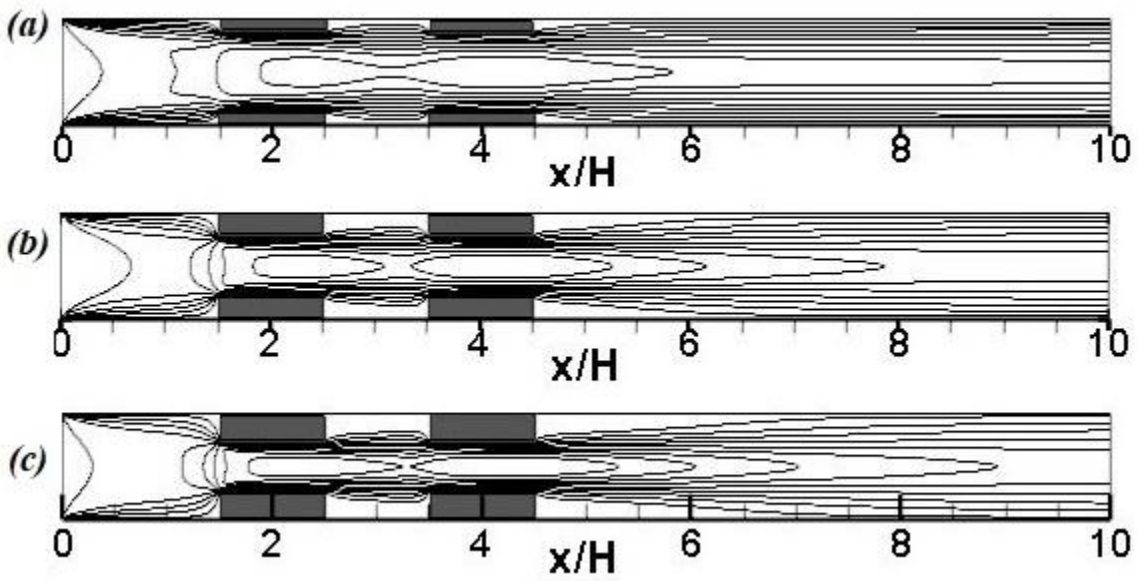

Figure 9: Velocity contours for Re=250: a) 2h/H=0.2, b) 2h/H=0.4, c) 2h/H=0.5.

The temperature field allows us to understand the effect of this variation in the constricted ratio in order to find the best way to rise the heat exchange between the channel wall and the studied fluid (see fig.10). When the constriction ratio increases up to 0.5, the heat transfer becomes more prevails in comparizon to low ratios.

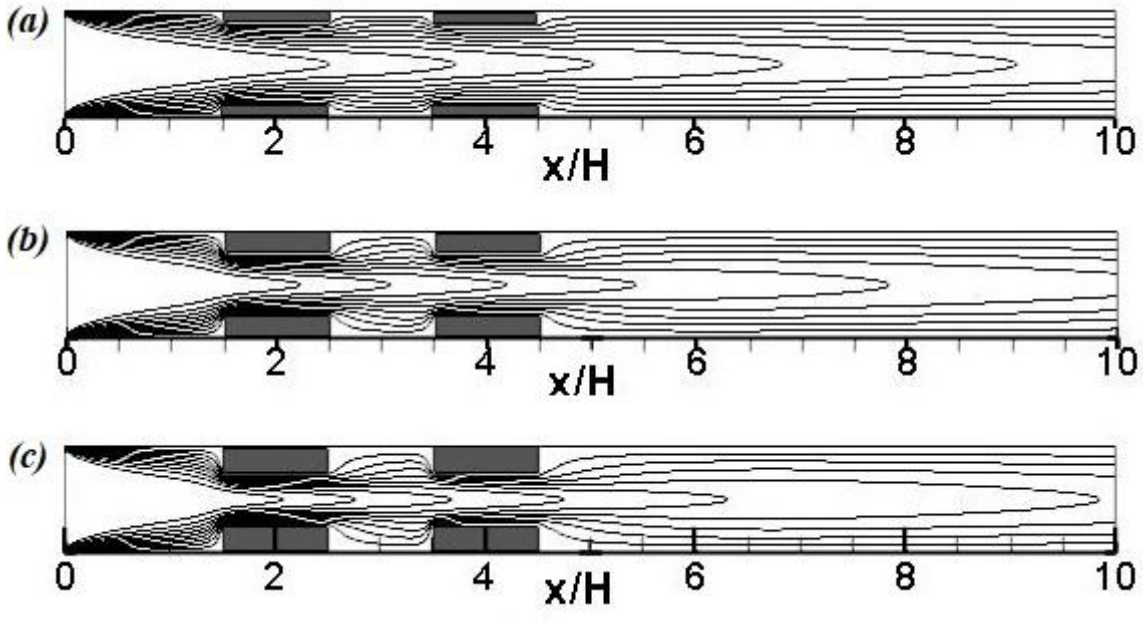

Figure 10: temperature field for Re=250: a) 2h/H=0.2, b) 2h/H=0.4, c) 2h/H=0.5.

To confirm the interpretation of the previously discussed results, numerical calculations of the average number of Nusselt <Nu> are taken into account for the lower channel wall (see fig.11). The increase in the number of Reynolds causes an increase in the average number of Nusselt, which means that the heat exchange becomes more important. The fluid approaches the upper wall and forms a recirculation zone in the lower wall, which explains the increase in <Nu> for Re = 250 contrary to what we found for Re = 300.

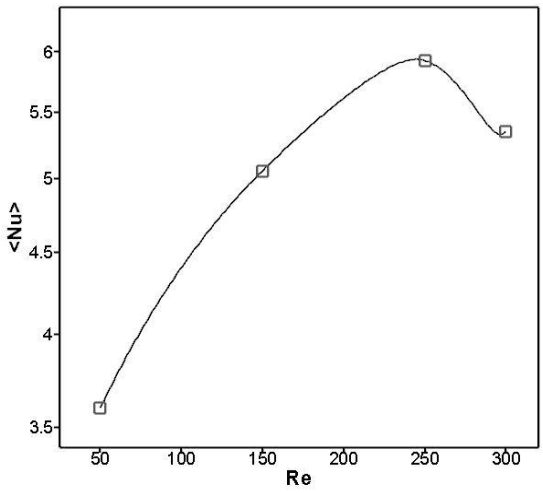

Figure 11: Average Nusselt number for 2h/H=0.6.

Conclusion.

This paper shows that Lattice's Boltzmann method using a double MRT scheme effectively simulates fluid flow and heat transfer in complex geometries. The obtained results allow us to conclude that the presence of the constricted part have an improvement of the heat transfer by convection between the fluid and the channel walls. Furthermore, to have an ideal cooling, it is necessary to use a fairly average velocity for the incoming fluid in order to avoid the recirculation zone behind each constricted part, and increase the heat transfer enhancement. One can noted for our secondly study that the variation of the constriction ratio has a considerable effect on the heat transfer between the walls and the fluid. When the constriction ratio is less than 0.4, the heat transfer is more intense compared to a ratio higher than this value

References.

[1] A. Bar-Cohen, A. D. Kraus, S. F. Davidson, Thermal frontiers in the design and packaging of microelectronic equipment, J. Mechanical Engineering, Vol. 105,Issue 5, pp. 530-539, 1983.

[2] A. D. Kraus, A. Bar-Cohen, A. A. Wative, Cooling electronic equipment. Prentice-Hall, 1965.

[3] A.-R.A. Khaled, K. Vafai. Heat transfer enhancement through control of thermal dispersion effects. International Journal of Heat and Mass Transfer,, vol. 48, no 11, pp. 2172-2185, 2005.

[4] T.J. Young, K.Vafai, Convective cooling of a heated obstacle in a channel, International Journal of Heat and Mass Transfer, vol.41,no 20, pp. 3131-3148,1998.

[5] A. A. Alamyane, A. A. Mohamad, Simulation of forced convection in a channel with extended surfaces by the lattice Boltzmann method. Computers & Mathematics with Applications, vol. 59, no 7, pp. 2421-2430, 2010.

[6] M.A. Moussaoui, A. Mezrhab, H. Naji, A computation of flow and heat transfer in a plane channel with three heated cylinders in a vee shape by a double distribution MRT thermal lattice Boltzmann model, International Journal of Thermal Sciences, Vol. 50, pp. 1532 – 1542, 2011.

[7] M. M. Pirouz, M. Farhadi, K. Sedighi, et al, Lattice Boltzmann simulation of conjugate heat transfer in a rectangular channel with wall-mounted obstacles. Scientia Iranica, vol. 18, no 2, pp. 213-221, 2011.

[8] D.H. Rothman, S. Zaleski, Lattice-gas cellular automata: simple models of complex hydrodynamics. Cambridge University Press, 2004.

[9] P. L. Bhatnagar, E.P. Gross, M. Krook, A model for collision processes in gases. I. Small amplitude processes in charged and neutral one-component systems. Physical review, vol. 94, no 3, pp. 511, 1954.

[10] A. A. Mohamad, Lattice Boltzmann method: fundamentals and engineering applications with computer codes. Springer Science & Business Media, 2011.

[11] D. d'Humières, Multiple–relaxation–time lattice Boltzmann models in three dimensions. Philosophical Transactions of the Royal Society of London A: Mathematical, Physical and Engineering Sciences, vol. 360, no 1792, pp. 437-451, 2002.

[12] A. Tarokh, A.A. Mohamad, L. Jiang, Simulation of conjugate heat transfer using the lattice Boltzmann method. Numerical Heat Transfer, Part A: Applications,, vol. 63, no 3, pp. 159-178, 2013.

[13] M. A. Moussaoui, J. Mohamed, A. Mezrhab, H. Naji, Computation of heat transfer and fluid flow in an obstructed channel using lattice Boltzmann method. Engineering Computations 27, no. 1: pp. 106-116, 2010.

[14] A. Mezrhab, M. Bouzidi, P. Lallemand, Hybrid lattice Boltzmann finite-difference simulation of convective flows, Computers and Fluids, Vol. 33, pp. 623-641, 2004.

[15] H. Y. Lai, S. C. CHang. W. L. Chen, Lattice Boltzmann Method for Turbulent Heat Transfer in Wavy Channel Flows. In : Proceedings of World Academy of Science, Engineering and Technology. World Academy of Science, Engineering and Technology (WASET). pp. 814, 2013.

[16] M. M. Keshtkar, M. Ghazanfari, Numerical investigation of fluid flow and heat transfer inside a 2D enclosure with three hot obstacles on the ramp under the influence of a magnetic field. Engineering, Technology & Applied Science Research, vol. 7, no 3, pp. 1647-1657, 2017.

[17] Z. Li, M. Yang, Y. Zhang, Double MRT thermal lattice Boltzmann method for simulating natural convection of low Prandtl number fluids. International Journal of Numerical Methods for Heat & Fluid Flow, vol. 26, no 6, pp. 1889-1909, 2016.

[18] M. A. Moussaoui, M. Jami, A. Mezrhab,. Lattice Boltzmann simulation of convective heat transfer from heated blocks in a horizontal channel. Numerical Heat Transfer, Part A: Applications, vol. 56, no 5, pp. 422-443, 2009.

[19] S. Gokaltun, G. S. Dulikravich, Lattice Boltzmann computations of incompressible laminar flow and heat transfer in a constricted channel. Computers & Mathematics with Applications, vol. 59, no 7, pp. 2431-2441, 2010.

[20] A. Mezrhab, M.A. Moussaoui, M. Jami, H. Naji, M. Bouzidi, Double MRT thermal lattice Boltzmann method for simulating convective flows, Physics Letters A, Vol. 374, pp. 3499–3507, 2010.

[21] Q. Zou et X. He, On pressure and velocity boundary conditions for the lattice Boltzmann BGK model. Physics of fluids, vol. 9, no 6, pp. 1591-1598, 1997.

[22] S. Rodríguez-Romo, O. Ibañez-Orozco, Two-Dimensional Lattice Boltzmann for Reactive Rayleigh–Bénard and Bénard–Poiseuille Regimes. Entropy, vol. 17, no 10, pp. 6698-6711,2015.